KeAi
CHINESE ROOTS
GLOBAL IMPACT

Contents lists available at ScienceDirect

Petroleum Science

journal homepage: www.keaipublishing.com/en/journals/petroleum-science



Synthesis kinetics of B-COPNA resin monitored by the transformation of functional groups using *in-situ* FTIR spectroscopy



Yuan-Qin Zhang ^{a,1}, Ling-Rui Cui ^{a,1}, Hong-Yan Shen ^a, Jun-Ping Shen ^{a,b}, Hong-Fang Ma ^a, Jun Xu ^{a,c}, Fa-Hai Cao ^{a,c,*}

- ^a School of Chemical Engineering, East China University of Science and Technology, Shanghai, 200237, China
- ^b Department of Energy and Chemical Engineering, Aksu Industry Polytechnic College, Aksu, 842000, Xinjiang, China
- c Large Industrial Reactor Engineering Research Center of Ministry of Education, East China University of Science and Technology, Shanghai, 200237, China

ARTICLE INFO

Article history: Received 16 September 2024 Received in revised form 14 April 2025 Accepted 9 June 2025 Available online 14 June 2025

Edited by Min Li

Keywords: Ethylene tar light fraction B-COPNA resin In-situ FTIR Synthesis kinetics

ABSTRACT

B-COPNA resin, synthesized from the light fraction of ethylene tar (ETLF), is a superior precursor of the carbon materials. An in-depth understanding of the COPNA resin preparation process and strict control of crosslinking degree are crucial for controlling carbon materials performance. Therefore, the synthesis kinetics of B-COPNA resin prepared from ETLF was investigated using *in-situ* FTIR in this work. The synthesis kinetic models of B-COPNA resin were established for the first time. To express the kinetic model, the concentration changes of C-H in aromatic rings and O-H in PXG monitored by *in-situ* FTIR were selected as two indicators to calculate concentration of other compounds and describe the synthesis kinetics. Then confirmatory experiments were conducted, and the ρ^2 (>0.9900), F-values (>10F_{0.05}) and parameter errors (below 3%) of kinetic models verify that concentration changes of C-H and O-H can be used to describe synthesis kinetics of B-COPNA resin. Based on the results of confirmatory experiments, the synthesis kinetic model of B-COPNA resin in the ETLF system is established successfully using concentration changes of O-H as an indicator, whose appropriateness and feasibility are proved by the ρ^2 (0.9960) and F-values (>10F_{0.05}). These models could accurately describe the synthesis rate of B-COPNA resin.

© 2025 The Authors. Publishing services by Elsevier B.V. on behalf of KeAi Communications Co. Ltd. This is an open access article under the CC BY-NC-ND license (http://creativecommons.org/licenses/by-nc-nd/4.0/).

1. Introduction

With the continuous growth of the global ethylene production capacity, mainly produced from the steam cracking process of naphtha, the resulting output of ethylene tar (ET) as the byproducts from this process has also increased, accounting for approximately 10%–15% of ethylene output (Chen et al., 2023; Fujitsuka et al., 2024; Guo et al., 2023; Liu et al., 2020; Muñoz and Weidema, 2024). The heavy fraction of ET with a high boiling point (>260 °C) is a valuable resource for producing carbon materials, including isotropic pitch (Ge et al., 2016; Liang et al.,

2020; Liu et al., 2018b, 2018c, 2020; Shi et al., 2019a), mesophase pitch (Cheng and Song, 2012; Ge et al., 2016), carbon fiber (Liu et al., 2018c; Özsin et al., 2019; Shi et al., 2019a, 2019b), needle coke (Yu et al., 2022) and so on. In contrast, the utility of light fraction in ET (ETLF, boiling point <260 °C), predominantly consisting of aromatic with 1–2 rings, remains limited. Consequently, improving the efficient utilization of ETLF is of paramount importance.

In our previous study (Shen et al., 2024), the ETLF was used to synthesize the B-stage condensed polynuclear aromatic (B-COPNA) resin, which is a carbon material precursor with excellent properties, consisting of polycyclic aromatic hydrocarbons connected by methylene or methine. The exceptional properties of B-COPNA resin such as superb adhesion, great heat resistance, and processability render it great potential for producing carbon materials and a good application prospect (Fang et al., 2022; Lin et al., 2010b; Ota et al., 1989; Ōtani et al., 1986; Shi et al., 2012; Tanemura et al., 2011; Wu et al., 2012, 2013; Zhang et al., 2015). For example,

^{*} Corresponding author.

E-mail address: fhcao@ecust.edu.cn (F.-H. Cao).

Peer review under the responsibility of China University of Petroleum (Beijing).

¹ These authors contributed equally to this work and should be considered cofirst authors.

COPNA resin could be utilized to fabricate the carbon spheres exhibiting excellent sphericity degree and thermal properties (Lin et al., 2010a), and to develop the carbon molecular sieving membrane for separating gas (Kusakabe et al., 1998). Liu and colleagues (Liu et al., 2014; Wang et al., 2016) utilized phenol and 1,4benzenedimethanol as raw material to synthesize the soluble COPNA resin, which was served as the foundational material for the preparation of the carbon foams through allylation with allyl chloride, curing with 4,4-bismaleimidodiphenyl methane (BDM) and subsequent high-temperature pyrolysis. The resulting carbon foams exhibited relatively low thermal conductivity and superior compressive strength. Wu et al. (2014) significantly enhanced the heat resistance and adhesive of the meltable COPNA resin by adding the bisphenol epoxy resin of 5%. The prepared electric motor brushes using modified resin as the binder possessed superior characteristics including low electrical resistivity and excellent mechanical properties. These studies highlight the immense application value of B-COPNA resin. However, most studies related to the COPNA resin mainly focused on the three aspects, including investigation of novel raw materials, optimization of preparation conditions and application of resin products. The effect of different operation conditions on the synthesis rate and reaction extent has not been investigated during the synthesis of COPNA resin.

In addition, some studies (Liu et al., 2018a, 2018b, 2020, 2022, 2023; Wang et al., 2019) explored the effect of different reaction extent (or crosslinking degree) on properties of products during the pitch preparation process from heavy aromatic oil, achieving an effective and controllable transformation from the aromatic hydrocarbons (AHCs) into carbon materials with excellent properties. These research results inspired us that the studying of reaction extent and reaction rate is significantly important and necessary for regulating performance of final products. Moreover, the synthesis process of COPNA resin was proved to be a tandem reaction by the DFT calculation in our previous work (Shen et al., 2024). Thus, it is significantly important to control the reaction degree during the B-COPNA resin synthesis, necessitating an indepth understanding of the synthesis features and strict control of the crosslinking degree throughout the B-COPNA preparation process. Therefore, the synthesis kinetics of B-COPNA resin prepared using ETLF and PXG were investigated in this work.

During the studying process of kinetic, the analytical instruments (such as UV-visible and FTIR spectroscopy) were applied to measure the change of component in the reaction system (e.g. concentration (Ahmad et al., 2023; Ahmad et al., 2024), intensity of functional groups (Xing et al., 2020)), in order to describe the reaction kinetic model and calculate the model's parameters. In our reaction system, the synthesis essence of B-COPNA resin is an electrophilic substitution reaction as demonstrated by our previous work (Shen et al., 2024). During the synthesis process, the hydrogen in aromatic rings (C-H) reacts with the -OH in PXG, generating H₂O. Thus, to study the reaction kinetics of B-COPNA resin, an approach has been proposed to select the concentration changes of C-H and -OH as two indicators for monitoring the reaction process and describing the kinetic model in the present work. Typically, the reaction extent could be inferred from the alterations in the concentration of these groups which can be detected using the Fourier Transform Infrared Spectrometer (FTIR) (Cheng et al., 2018; Shi et al., 2012; Tokunaga et al., 2024; Xing et al., 2020). However, the conventional off-line FTIR, a common technique for identifying the groups in samples, generally requires complex sample pretreatment (e.g. removing catalyst, drying samples, etc.). This not only increases the timeconsuming and workload but also limits the ability to accurately capture the real-time concentration changes of these groups

within the reaction system. Consequently, the credibility and accuracy of data are low. To tackle these limitations, the potential of in-situ FTIR has been developed in recent years as a powerful kinetics research technique, which can continuously monitor the reaction process and provide real-time information on the concentration changes of specific groups within the reaction system (Niu et al., 2016; Ye et al., 2022; Zhang et al., 2016). Tomazett et al. (2017) investigated the polymerization rate and conversion degree based on the absorption intensity change of specific groups, which are observed using in-situ FTIR equipped with ATR accessory. Similarly, Ye et al. (2022) studied the reaction mechanism of Paal-Knorr reaction and identified the system components using in-situ FTIR. The FTIR data were analyzed quantificationally by combining with other treatment techniques and the kinetic model was established finally. With the aid of the in-situ FTIR equipped reaction pool with a CaF₂ window and MCT detector, Xing et al. (2020) also collected the group intensity variation with temperature and researched the reaction mechanism during the cracking oxidation process of polypropylene. Importantly, the intensity changes of functional groups detected by the in-situ FTIR can be used to established reaction kinetic models, such as oxidation reaction kinetics of coal (Zhang et al., 2016). Based on these studies, an approach for researching the synthesis kinetics of B-COPNA resin, through in-situ FTIR equipped with a reaction pool, was proposed in the present work.

In this work, the elemental reactions that may occur during the synthesis process of B-COPNA resin were elucidated based on the reaction mechanism in our previous work for the first time (Shen et al., 2024). Furthermore, the synthesis kinetic model of B-COPNA resin was derived, expressed in the kinetic model of PXG consumption. Then two indicators (including concentration changes of C-H and O-H) were proposed to investigate the synthesis kinetics of B-COPNA resin and the in-situ FTIR equipped with a reaction pool was employed to monitor in real-time the concentration changes of functional groups. To illustrate the feasibility of two indicators for describing the kinetics, the confirmation experiments using 1-ethylnaphthalene (EtNp) as raw materials were conducted. Combining the fourth-order Runge-Kutta with the Levenberg-Marquardt method, the kinetic models are calculated and their parameters are optimized and estimated. Proved by the statistic test, the concentration changes of C-H and O-H can be used to describe the synthesis kinetic of B-COPNA resin. Finally, the kinetic model of PXG consumption is established successfully, which is conducive to the regulation and description of the synthesis rate of B-COPNA resin by changing experimental conditions. Meanwhile, this study provides an efficient approach to investigate the crosslinking reaction kinetics of B-COPNA resin using ETLF and PXG as raw materials.

2. Experimental

2.1. Materials and reagents

The PXG (98%), PTS (99%), 1-ethylnaphthalene (99%) were provided by Macklin. The ETLF was supplied by ethylene cracking unit in Sinopec Maoming Petrochemical Co. Ltd.

2.2. In-situ FTIR apparatus

Aiming to acquire the intensity changes of the specific functional groups in real-time within the system, the *in-situ* FTIR apparatus equipped with a reaction pool was designed, as shown in Fig. 1. All spectra were recorded in the range of 4000–1000 cm⁻¹ using 32 scans at a resolution of 4 cm⁻¹. Firstly, the raw materials, crosslinking agent, and catalyst were placed into the reaction pool,

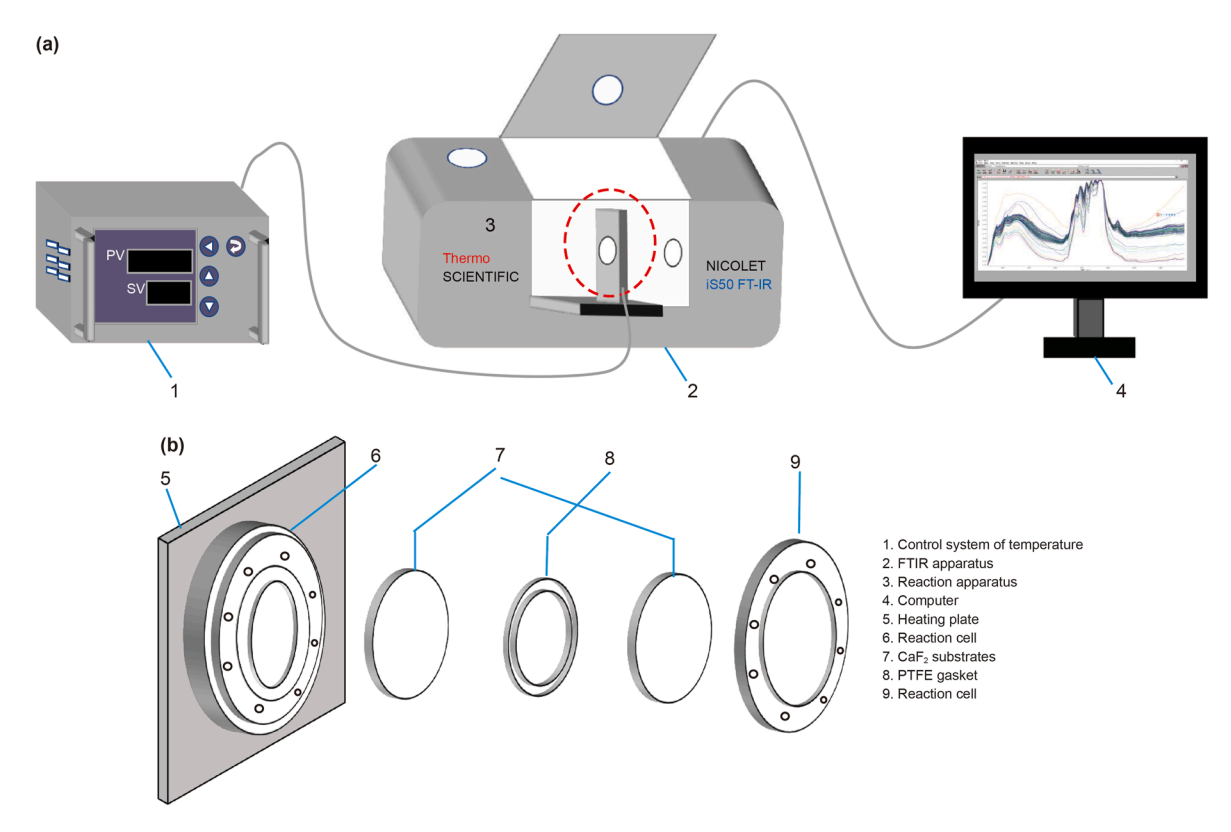


Fig. 1. Schematic depiction of (a) in-situ FTIR apparatus and (b) reaction pool.

as shown in Fig. 1(b). The reaction apparatus was then placed within the infrared detection device to collect intensity changes of functional groups in the system under various conditions. By designing the different experiment conditions, kinetic data regarding B-COPNA resin preparation could be obtained.

2.3. Relationship construction of absorbance-concentration of reactants

The synthesis mechanism of B-COPNA resin studied in our previous work indicates that the C–H (3040 cm $^{-1}$) in the aromatic rings would react with the –OH (3500 cm $^{-1}$) in PXG, generating H₂O (Shen et al., 2024), which results in gradually decrease of the absorption intensity of functional groups in FTIR as the time increased, as shown in Fig. 2. Therefore, when the in-situ FTIR was employed to track the reaction extent, an approach of selecting intensity changes of both O–H and C–H as indicators to monitor the reaction extent in this work was proposed. Additionally, the actual contents investigated in kinetic models are the concentration influence of compounds on the reaction rate. Thus, to conveniently and quickly convert the intensity changes of functional groups into concentration, the relationship of reactants concentrationabsorbance should be constructed.

The experiments for constructing the concentrationabsorbance relationships of C–H and O–H were conducted in the *in-situ* FTIR apparatus. Firstly, the solution with different mass ratios of PXG to oil, including 1:1, 1:2, 1:3, 1:4, 1:5 and 1:6, were prepared. Then, the concentrations of C–H and O–H in the system were calculated according to the mass ratio of oil to PXG. Finally, the intensities of C–H in oil and O–H in PXG were measured in the

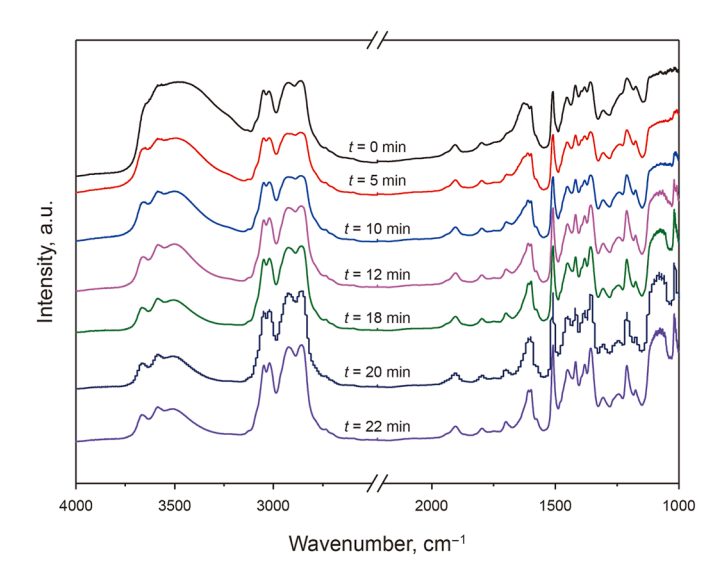
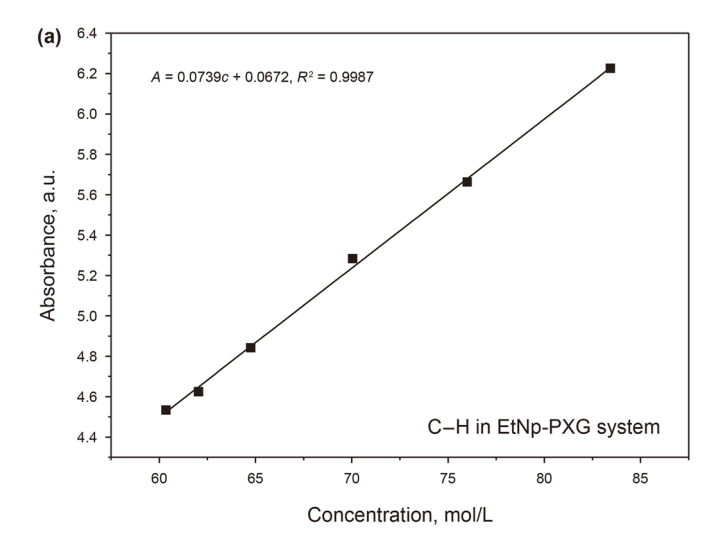
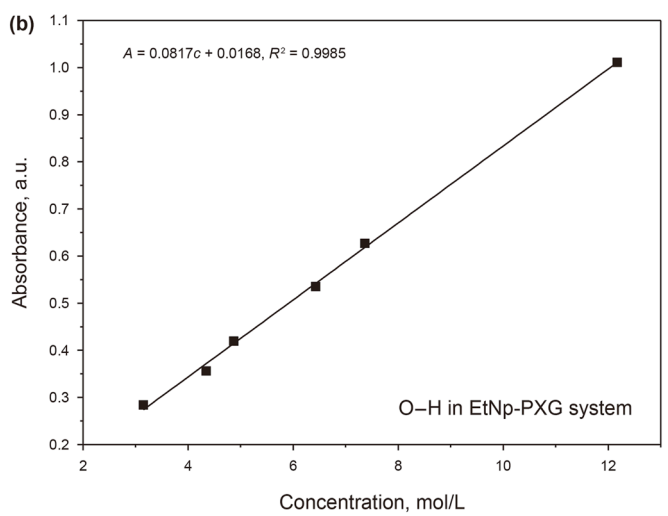


Fig. 2. *In-situ* FTIR spectra of functional group variation with time during the synthesis process of B-COPNA resin (the reaction condition is i = 1:2.5, T = 160 °C, cat. = 3%).

in-situ FTIR apparatus, all experiments were carried out repeatedly three times to reduce experimental errors. The relationship curves of concentration-absorbance in the different systems are shown in Fig. 3 when the intensity change of C–H or O–H was selected as the measurement indicator, the symbols *A* and *c* in these equations are absorbance and molar concentration in unit of mol/L, respectively.





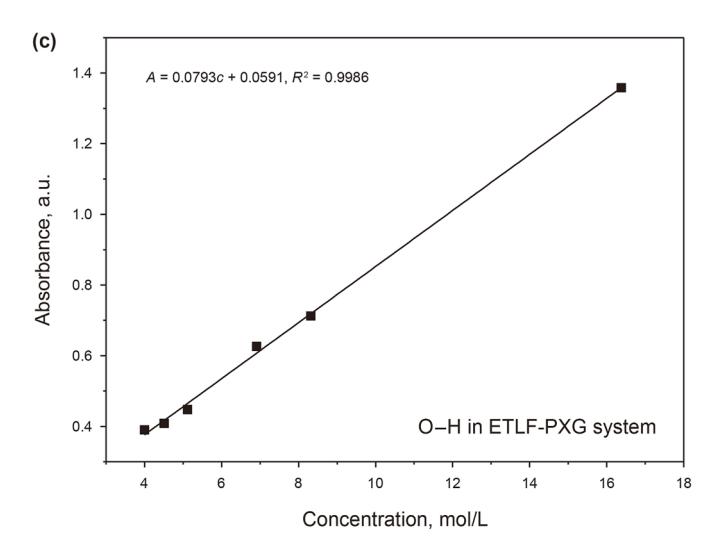


Fig. 3. Relationship curves of concentration-absorbance in different systems.

3. Establishment of kinetic model

3.1. Establishment of the ETLF-PXG model

According to the reaction mechanism (Shen et al., 2024), the elementary reactions that may occur during the synthesis of B-COPNA resin are shown in Eqs. (1)–(6), where the K_i (i=1–6) denotes the rate constant of each step. The molecular structures involved in these formulas are illustrated in Fig. 4, in which the ETLF presents the average molecular structure of ethylene tar light fraction. The subsequent cross-linking reaction pathway follows a similar pattern.

$$PTS \xrightarrow{K_1} PTS^{\ominus} + H^+ \tag{1}$$

$$PXG + H^{+} \xrightarrow{K_2} PXG - H \tag{2}$$

$$PXG - H \xrightarrow{K_3} PXG^+ + H_2O \tag{3}$$

$$PXG^{+} + ETLF \xrightarrow{K_4} COPNA - H$$
 (4)

$$COPNA - H \xrightarrow{K_5} COPNA + H^+$$
 (5)

$$PTS^{\ominus} + H^{+} \stackrel{K_6}{\rightarrow} PTS \tag{6}$$

To further deduce the synthesis kinetic models of B-COPNA resin, the following five hypotheses are given: 1) The B-COPNA resin is synthesized in a liquid phase system at a minimum reaction temperature of 140 °C. There is no accumulation of H_2O and no product adsorption on the catalyst surface during the synthesis process; 2) The collisions between the reactants are considered completely elastic, with no energy loss during the synthesis process; 3) Due to the high energy and extreme instability of the transition state, the accumulation of intermediate products generated during the synthesis process is ignored; 4) The effect of electron density in aromatic rings on the reaction rate is not considered in the model; 5) The preparation process of B-COPNA resin is irreversible, and the side reactions are not considered.

Based on the aforementioned hypotheses and the reaction equilibrium relationship of elementary reactions, the rate constants can be expressed in terms of the component molar concentration in the reaction system, as shown in Eqs. (7)–(12), where the symbol "[]" denotes the molar concentration in units of mol/L.

$$K_1 = \frac{[PTS^{\ominus}][H^+]}{[PTS]} \tag{7}$$

$$K_2 = \frac{[\mathsf{PXG} - \mathsf{H}]}{[\mathsf{PXG}][\mathsf{H}^+]} \tag{8}$$

$$K_3 = \frac{[PXG^+][H_2O]}{[PXG - H]}$$
 (9)

$$K_4 = \frac{[\text{COPNA} - \text{H}]}{[\text{PXG}^+][\text{ETLF}]} \tag{10}$$

$$K_5 = \frac{[\text{COPNA}][\text{H}^+]}{[\text{COPNA} - \text{H}]} \tag{11}$$

Fig. 4. Molecular structures of compounds involved in the reaction process.

$$K_6 = \frac{[PTS]}{[PTS^{\ominus}][H^+]} \tag{12}$$

According to the mechanism proposed in our previous work (Shen et al., 2024), the electron of hydroxyl in PXG is donated to the proton core generated from PTS, resulting in the formation of PXG–H. The highest free energy barrier of 37.4140 kcal/mol is required in this step throughout the entire synthesis process. Therefore, Eqs. (2) and (3) are identified as the rate-determining step. This indicates that the crosslinking degree during the B-COPNA resin synthesis process is controlled by the consumption rate of PXG. Consequently, the synthesis kinetic model of B-COPNA resin can be expressed by the kinetic model of PXG consumption. The relationships between component concentration and rate constants are presented in Eqs. (13)–(16).

$$[PXG - H] = K_2[PXG][H^+]$$
(13)

$$[PXG^{+}] = \frac{K_{3}[PXG - H]}{[H_{2}O]}$$
 (14)

$$[COPNA - H] = K_4[PXG^+][ETLF]$$
(15)

$$[H^{+}] = \frac{K_{5}[COPNA - H]}{[COPNA]}$$
 (16)

Therefore, the kinetic model of PXG consumption (denoted as ETLF-PXG model) is derived and shown in Eq. (17) according to the above equations, where $K_{\rm ETLF}=K_{\rm 2_{\rm ETLF}}K_{\rm 3_{\rm ETLF}}K_{\rm 4_{\rm ETLF}}K_{\rm 5_{\rm ETLF}}$.

$$r_{2_{\text{ETLF}}} = -\frac{dC_{\text{PXG}}}{dt} = K_2[\text{PXG}][\text{H}^+] = K_{\text{ETLF}} \frac{[\text{PXG}][\text{ETLF}]}{[\text{COPNA}]} \frac{[\text{PXG} - \text{H}]}{[\text{H}_2\text{O}]}$$
(17)

3.2. Establishment of the EtNp-PXG model

The synthesis mechanism of B-COPNA resin indicates that concentration changes of the C-H bond in aromatic rings and O-H in PXG could theoretically reflect the crosslinking degree of B-COPNA resin. However, ETLF with complex composition contains some aromatic hydrocarbons with low reactivity that cannot react with PXG, so it is doubtful to adopt the concentration change of

C–H as an indicator to describe the kinetic model of PXG consumption in ETLF-PXG reaction system.

To verify the feasibility of two indicators (including concentration changes of C–H and O–H) for describing the kinetic model, the confirmation experiments using 1-ethylnaphthalene (EtNp) as raw materials instead of ETLF are conducted. These results could provide a basis for selecting the intensity changes of O–H in PXG as an indicator to monitor reaction extent in the ETLF reaction system.

Considering the similar reaction mechanism between EtNp and ETLF, the kinetic model of PXG consumption in the EtNp system (denoted as EtNp-PXG model) is presented in Eq. (18), where $K_{\rm EtNp} = K_{2_{\rm EtNp}} K_{3_{\rm EtNp}} K_{4_{\rm EtNp}}$, the EtNp denotes the reaction system selecting EtNp as raw materials.

$$r_{2_{\text{EtNp}}} = K_{\text{EtNp}} \frac{[PXG][EtNp]}{[COPNA]} \frac{[PXG - H]}{[H_2O]}$$
(18)

4. Results and discussion

4.1. Evaluation and optimization of the EtNp-PXG model

To investigate the relationship between experimental factors and the EtNp-PXG model, including the ratio of crosslinking agent to EtNp (*i*), reaction temperature (*T*), catalyst content (cat.), orthogonal experiments with three factors and four levels were designed for obtaining the intensity variation of C–H and O–H in the reaction system with reaction time. Experimental data was collected at 5-min intervals for a total of 5 h. The orthogonal experiment design and results are presented in Table 1, and more data are shown in Table S1 and Table S2 in Supplementary material

According to the reaction mechanism and main characteristics of B-COPNA resin synthesis, the concentration of PXG^+ increases as the concentration decrease of O–H or C–H. Thus, the concentration change of O–H or C–H can be converted into PXG^+ concentration in the system. Subsequently, the concentrations of other compounds in the system can be determined using the quantitative relationship of elementary reactions, as shown in Eq. (19). The $C_{PXG,0}$ and $C_{EtNp,0}$ in Eq. (19) represent the initial concentration of PXG and EtNp, respectively.

Table 1
Concentration changes of C-H and O-H in the EtNp-PXG reaction system.

No.	i	T, °C	Cat., %	Indicator	C_{PXG}^{+} at different time, mol/L		
					5 min	10 min	15 min
1	1:2.0	160	2	O-H	2.938	4.950	7.606
				C–H	27.638	49.715	62.250
2	1:2.0	170	3	O–H	3.265	5.923	8.034
				C–H	39.823	55.652	68.223
3	1:2.0	180	4	O–H	4.433	8.669	10.408
				C–H	26.705	60.152	79.622
4	1:2.0	190	5	O–H	4.845	7.379	9.863
				C–H	44.372	58.471	68.588
5	1:2.5	160	3	O–H	2.908	3.500	5.961
				C–H	15.123	18.200	30.998
6	1:2.5	170	2	O–H	3.490	4.910	5.020
				C–H	23.312	25.492	31.250
7	1:2.5	180	5	O–H	2.020	4.284	6.059
				C–H	10.577	22.435	31.730
8	1:2.5	190	4	O–H	2.693	5.263	7.111
				C–H	13.950	27.266	36.841
9	1:3.0	160	4	O–H	1.145	1.469	2.338
				C–H	5.487	7.042	9.208
10	1:3.0	170	5	O–H	1.124	2.979	3.834
				C–H	5.465	8.485	11.640
11	1:3.0	180	2	O–H	1.659	2.928	5.102
				C–H	1.398	7.572	11.140
12	1:3.0	190	3	O–H	2.575	5.549	5.635
				C–H	5.739	13.067	20.480
13	1:3.5	160	5	O–H	0.679	1.171	1.445
				C–H	1.765	2.464	3.400
14	1:3.5	170	4	O–H	1.203	1.717	2.255
				C–H	4.298	5.269	6.673
15	1:3.5	180	3	O–H	0.996	1.963	2.783
				C–H	3.688	5.951	7.566
16	1:3.5	190	2	O–H	2.845	3.253	4.122
				C–H	4.059	6.884	8.767

Note: The EtNp, PXG and PTS are used as raw material, crosslinking agent and catalyst, respectively.

$$[PXG] = C_{PXG,0} - dC_{PXG}$$

$$[EtNp] = C_{EtNp,0} - dC_{PXG}$$

$$[COPNA] = dC_{PXG}$$
(19)

Based on hypothesis 1) and hypothesis 3), the concentration effects of PXG–H and H_2O on the model can be neglected, thus the simplified model of Eq. (18) is presented as Eq. (20), where K_{EtNp} represents rate constant at the reaction temperature and can be obtained by calculating Eq. (21). K_a , E_b , and R in Eq. (21) are the preexponential factor, activation energy and molar gas constant, respectively. Then the consumption rate of PXG is acquired via integrating Eq. (20) using the fourth-order Runge-Kutta method, as shown in Eqs. (22)–(26).

$$r'_{2_{EtNp}} = K_{EtNp} \frac{[PXG][EtNp]}{[COPNA]}$$
 (20)

$$K_{\rm EtNp} = K_{\rm a} e^{\left(-\frac{F_{\rm b}}{RT}\right)} \tag{21}$$

$$y_{n+1} = y_n + \frac{h}{6}(K_1 + 2K_2 + 2K_3 + K_4)$$
 (22)

$$K_1 = f(x_n, y_n) \tag{23}$$

$$K_2 = f\left(x_n + \frac{h}{2}, y_n + \frac{h}{2}K_1\right)$$
 (24)

$$K_3 = f\left(x_n + \frac{h}{2}, y_n + \frac{h}{2}K_2\right)$$
 (25)

$$K_4 = f(x_n + h, y_n + hK_3)$$
 (26)

The model's accuracy was evaluated by the residual sum of squares (S_c), a target function of mathematical modeling, as shown in Eq. (27), where $C_{PXG^+_{cal.i}}$ and $C_{PXG^+_{exp.i}}$ represent the calculated and experimental value of PXG^+ concentration, respectively. Besides, the model parameters are estimated using the Levenberg-Marquardt method, which integrates the advantages of the Newton method and gradient descent method, offering good numerical stability. When setting algorithm parameters, the pattern, combining Levenberg-Marquardt with general global optimization, was selected. The calculation process of model's parameters is shown as Scheme 1.

$$S_{c} = \sum_{i=1}^{N_{\text{exp}}} \left(C_{\text{PXG}_{\text{cal},i}^{+}} - C_{\text{PXG}_{\text{exp},i}^{+}} \right)^{2}$$
 (27)

After estimating and optimizing the model parameters, the model correlation coefficient (R \ll 0.9) was obtained, which indicates the matched degree between the model and experiment results is extremely poor. Therefore, the model shown in Eq. (20) should be corrected based on the experiment data to accurately describe the reaction rate of the system.

According to hypothesis 5), the crosslinking reaction is irreversible, thus the reaction rate is only dependent on the reactant concentration. Consequently, the concentration of the COPNA resin ([COPNA]) in Eq. (20) would be disregarded. In addition, the influences of experiment factors (including i, T and cat.) on the synthesis of the B-COPNA resin have been investigated in our previous work (Shen et al., 2024), so the impacts of these factors on the synthesis kinetics of the B-COPNA resin should be considered. The revised model is given in Eq. (28), where the m, n, o, p and q are constant.

$$r_{2_{\text{EtNp}}}^{"} = K_{\text{EtNp}}[PXG]^{m}[EtNp]^{n} i^{o} T^{p} \text{Cat.}^{q}$$
(28)

The fourth-order Runge-Kutta method was employed to calculate Eq. (28) and the model parameters were estimated using the Levenberg-Marquardt method. Following the estimation and optimization of model parameters, the kinetic model of PXG consumption in the EtNp system can be described by Eqs. (29) and (30)

The kinetic model established by using the O–H concentration change in PXG:

$$r_{2_{\text{EtNp}}}'' = 24.574 \exp\left(-\frac{54627}{RT}\right) C_{\text{PXG}}^{0.134} C_{\text{EtNp}}^{4.101} i^{7.200}$$

$$T^{0.142} \text{Cat}^{0.120}$$
(29)

The kinetic model established by using the C–H concentration change in EtNp:

$$r''_{2_{\text{EtNp}}} = 23.885 \exp\left(-\frac{53353}{RT}\right) C_{\text{PXG}}^{0.133} C_{\text{EtNp}}^{3.245} i^{7.091}$$

$$T^{0.139} \text{Cat.}^{0.119}$$
(30)

To evaluate the reasonability and applicability of the model, the statistical test of the model is conducted. The F and ρ^2 are calculated by Eqs. (31) and (32), respectively. The symbols $M_{\rm p}$, N, $C_{\rm exp, \it j, \it i}$

Definition model parameters: K_a , E_b , m, n, o, p, q



Definition variables involved in the synthesis kinetic model of B-COPNA resin: $i,\ T,\ t_i,\ C_{\rm cat},\ C_{\rm PXG},\ C_{\rm oil},\ C_{\rm c}$



Definition function: input the synthesis kinetic model of B-COPNA resin



Define data: enter the value of the defined parameter



Input experiment data: including i, T, t_i , $C_{\text{cat.}}$, C_{PXG} , C_{oil} , C_{c} at different conditions



Algorithm settings: the Levenberg-Marquardt (LM) was selected and the calculation pattern was set as "standard (LM) + general global optimization"



Execute the algorithm and get the result

Scheme 1. The calculation process of parameters in model.

and $C_{\text{cal}, j}$ in these two formulas are respectively the number of model parameters, experiment numbers, experimental concentration values and calculated concentration values of PXG⁺. The statistical results are summarized in Table 2.

$$F = \frac{\left[\sum_{j=1}^{N_{\text{exp}}} \left(C_{\text{exp},j}\right)^{2} - \sum_{j=1}^{N_{\text{exp}}} \left(C_{\text{exp},j} - C_{\text{cal},j}\right)^{2}\right] / M_{\text{p}}}{\left[\sum_{j=1}^{N_{\text{exp}}} \left(C_{\text{exp},j} - C_{\text{cal},j}\right)^{2}\right] / (N_{\text{exp}} - M_{\text{p}})}$$
(31)

$$\rho^{2} = 1 - \sum_{j=1}^{N_{\text{exp}}} \left(C_{\exp,j} - C_{\text{cal},j} \right)^{2} / \sum_{j=1}^{N_{\text{exp}}} C_{\exp,j}^{2}$$
 (32)

As observed in Table 2, the F-values for both models are decuple higher than the critical value for 95% confidence level of the F-test (F_{0.05}) and the ρ^2 values exceed 0.9, which proves these two models (Eqs. (29) and (30)) are reasonable and applicable. This conclusion can be certified by the negligible deviation degree between the experimental values and calculated values of C^+_{PXG} , as shown in Fig. 5.

Table 2Results of the statistic test of the kinetic model.

Indicator	$M_{\rm p}$	$N_{\rm exp}$	F	ρ^2	F _{0.05}
О–Н	7	1152	39815.625	0.9959	2.01
C–H	7	1152	50204.930	0.9968	2.01

To verify that both Eq. (29) and Eq. (30) could describe the kinetic model of PXG consumption, the parameters of these two models are summarized in Table 3 and are compared with each other. The relative errors of various parameters, including K_a , E_b , m, o, p and q, are below 3%, except for n (20.87%), which could be ascribed to the unique structure of EtNp. Due to its enriched C–H structure, EtNp exhibits a higher concentration of C–H compared to O–H in the EtNp system. Consequently, when C–H concentration is used as the calculation indicator, a higher concentration of EtNp is obtained. This results in a slightly lower concentration change rate of EtNp in Eq. (30) compared to Eq. (29) due to the greater initial concentration on the reaction rate, as represented by parameter n in Eq. (30), is lower than that in Eq. (29).

The above findings illustrate that all parameters in Eqs. (29) and (30) have almost identical influences on the respective models. As a result, the kinetic model of PXG consumption in the synthesis system of B-COPNA resin can be effectively described using Eqs. (29) and (30). Specifically, the concentration changes of both C-H in aromatic rings and O-H in PXG can be used as indicators to describe the kinetic model of PXG consumption.

4.2. Evaluation and optimization of the ETLF-PXG model

The research results presented in subsection 4.1 have demonstrated the concentration changes of both C–H in aromatic rings and O–H in PXG can describe the synthesis kinetics of B-COPNA resin. However, due to the composition complexity of ETLF and the difficulty of concentration calculation as described in subsection 3.2, the concentration change of O–H in PXG is selected as an indicator in this section to construct the kinetic model of PXG consumption in the ETLF system.

To elucidate the relationships between experimental factors and the ETLF-PXG model, including the ratio of crosslinking agent to ETLF (i), reaction temperature (T), and catalyst content (cat.), the single factor and orthogonal experiments were designed. The experiment design and results are shown in Table 4, and more data are shown in Table S3 in Supplementary material.

Based on the method and results in subsection 4.1, the corrected ETLF-PXG model can be obtained and presented in Eq. (33), the concentrations of other compounds in the ETLF system are calculated using Eq. (34), where the $C_{\rm PXG,0}$ and $C_{\rm ETLF,0}$ in Eq. (29) denote the initial concentration of PXG and ETLF, respectively.

$$r''_{2_{\text{ETLF}}} = K_{\text{ETLF}}[PXG]^m[\text{ETLF}]^n i^o T^p \text{Cat.}^q$$
(33)

$$[PXG] = C_{PXG,0} - dC_{PXG}$$

$$[ETLF] = C_{ETLF,0} - dC_{PXG}$$

$$[COPNA] = dC_{PXG}$$

$$K_{ETLF} = K_a e^{\left(-\frac{E_b}{RT}\right)}$$
(34)

The fourth-order Runge-Kutta method is employed to integrate Eq. (33), and the model parameters were estimated by the Levenberg-Marquardt method. The ETLF-PXG model is shown as Eq. (35) after estimating and optimizing the model parameters.

$$r''_{2_{\text{ETLF}}} = 41.277 \exp\left(-\frac{76125}{RT}\right) C_{\text{PXG}}^{3.102} C_{\text{ETLF}}^{1.428} i^{1.802}$$

$$T^{0.321} \text{Cat.}^{0.0855}$$
(35)

The statistics test results of the ETLF-PXG model are present in Table 5. The ETLF-PXG model's F-value is decuple higher than that of $F_{0.05}$, and the value of ρ^2 is 0.9960, exceeding 0.9000.

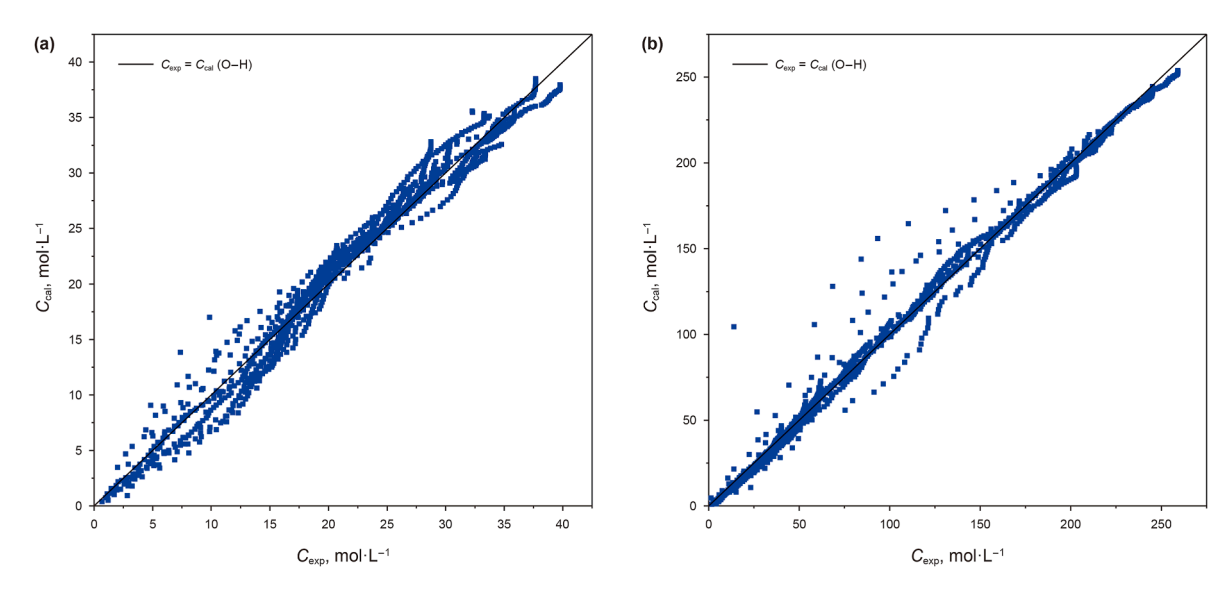


Fig. 5. Comparison of experimental and calculated values of C_{PXG}^{+} in the EtNp system.

Additionally, the experimental data and calculated data of C^+_{PXG} are closely distributed on the diagonal sides, as shown in Fig. 6. Above results indicate that the ETLF-PXG model is appropriate.

The ETLF-model, as presented by Eq. (35), reveals the significant influence of various operational conditions (including operation temperature, reaction time, ratio of crosslinking agent to oil, dosage of catalyst) on the synthesis rate of B-COPNA resin in the ETLF reaction system. As can be seen from this model, the exponents of C_{PXG} , C_{ETLF} and i are respectively 3.102, 1.428, and 1.802, they are greater than 1. This emphasizes that the concentrations of ETLF and PXG have a crucial effect on the synthesis rate of B-COPNA resin. All of the results could be explained in terms of the collision theory of chemical reactions. Namely, the number of molecules and the rate of collisions in the system increase as the concentration of ETLF and PXG in the system increases. Consequently, the PXG⁺ concentration increases, accelerating the reaction rate of the electrophilic substitution reaction between PXG⁺ and ETLF in the system. Therefore, there is a substantial influence of ETLF and PXG concentration on the ETLF-PXG model.

As to the exponent *T* and cat., their respective values of 0.3210 and 0.0855 denote a positive effect on the ETLF-PXG model. The positive impact of temperature can be attributed to the higher energy acquired by the reactants at higher temperatures, leading to a higher effective collision rate and accelerating reaction rate. The relatively low exponent for the catalyst illustrates that its influence on the reaction rate is minimal, this may be attributed to the fact that the catalyst is not actually involved in the reaction. The above research results of the ETLF-PXG model provide a

Table 3Model parameters of PXG consumption kinetic model in EtNp system.

Model	Indicator	K _a ^a	E _b , kJ/mol	m	n	0	p	q
Eq. (29)	О–Н	24.574	54.627	0.135	4.101	7.200	0.143	0.120
Eq. (30)	C-H	23.885	53.353	0.133	3.245	7.091	0.139	0.119
Relative	error. %	2.800	2.330	1.480	20.870	1.510	2.800	0.008

The unit of K_a in Eq. (29): $L^{3.236} \circ C^{0.143} \text{mol}^{-3.236} \text{min}^{-1}$. The unit of K_a in Eq. (30): $L^{2.378} \circ C^{0.139} \text{mol}^{-2.378} \text{min}^{-1}$.

reference for the actual industrial production of B-COPNA resin. According to this kinetic model, the operation parameters for preparation of B-COPNA resin, including reaction temperature, reaction time, ratio of crosslinking agent to oil and dosage of catalyst, could be optimized, and the synthesis rate could be controlled by adjusting the concentration of crosslinking agent and ETLF during the industrial production, improving the production efficiency and quality of B-COPNA resin. This is a crucial step toward the controlled preparation and properties of products. This work provides a research method for the synthesis kinetic of B-COPNA resin. Nevertheless, the obtained kinetic model is applicable to predict the synthesis rate of B-COPNA resin prepared from ethylene tar with methyl naphthalene as main component, while the applicability of this model for predicting other aromatics-enriched oils still to be examined.

Table 4Concentration changes of O–H in the ETLF-PXG reaction system.

No.	i	T, °C	Cat., %	C_{PXG}^+ of different time, mol/L			
				5 min	10 min	15 min	20 min
1	1:1.0	140	3	2.085	4.421	4.703	6.371
2	1:2.0	140	3	1.425	2.400	3.854	4.299
3	1:2.0	160	2	1.066	2.794	4.332	4.851
4	1:2.0	160	3	2.270	4.338	5.713	7.995
5	1:2.0	180	3	3.605	5.324	7.952	10.815
6	1:2.0	180	4	4.458	6.035	8.838	9.477
7	1:2.0	180	5	4.398	7.263	9.554	11.305
8	1:2.0	180	5.5	4.358	6.935	8.738	10.377
9	1:2.0	190	5	3.329	7.291	8.855	10.810
10	1:2.0	200	3	6.265	11.886	13.248	15.279
11	1:2.5	160	3	1.190	3.228	4.082	5.889
12	1:2.5	190	4	3.304	7.734	9.093	11.009
13	1:3.0	140	3	0.743	0.901	1.098	1.433
14	1:3.0	160	4	1.160	3.039	3.821	4.767
15	1:3.0	190	3	2.986	4.262	6.564	7.914
16	1:3.5	160	5	0.503	1.303	2.279	3.279
17	1:3.5	170	4	1.729	4.390	6.723	6.984
18	1:4.0	140	3	0.265	0.404	0.567	0.781

Note: The ETLF, PXG and PTS are used as raw material, crosslinking agent and catalyst, respectively.

Table 5Statistic results of the kinetic model in the ETLF-PXG system.

$M_{\rm p}$	$N_{\rm exp}$	F	ρ^2	F _{0.05}
7	1152	40501.906	0.9960	2.01

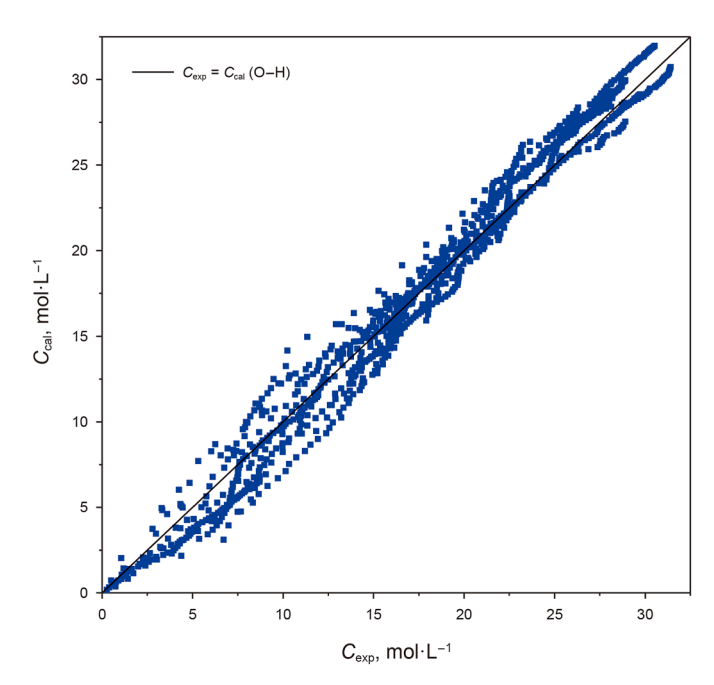


Fig. 6. Comparison of experimental and calculated $C_{\rm PXG}^+$ values in the ETLF-PXG system.

5. Conclusion

This study elucidates the elementary reactions involved in the synthesis process of B-COPNA resin for the first time according to its reaction mechanism. Based on this, the reaction kinetic model is derived and established. To effectively express the synthesis kinetic model of B-COPNA resin using reactant concentrations, two indicators (concentration changes of C-H and O-H) to describe the synthesis kinetic model are proposed. Combined with the fourthorder Runge-Kutta and the Levenberg-Marquardt method, the kinetic models and their parameters are calculated and estimated based on the *in-situ* FTIR data. The ρ^2 of the two models (established by using the concentration changes of C-H and O-H) from the confirmatory experiment are 0.9959 and 0.9968, respectively, which is higher than that of 0.9000. Additionally, the F-values of them exceed 10F_{0.05}. These results prove the feasibility and appropriation of the two models. Besides, the parameter errors of two models (below 3%) confirmed that concentration changes of both C-H in aromatic rings and O-H in PXG can be used to describe the synthesis kinetics of the B-COPNA resin. Based on the confirmatory experiment result, the kinetic model in the ETLF-PXG system is calculated and its paraments are estimated and optimized, the calculated values of C_{PXG}^+ were in great consistence with the experimental data and the results of ρ^2 (0.9960) and F $(>10F_{0.05})$ demonstrate the feasibility and appropriation of the kinetic model. According to this model, the influence of different operation parameters on the synthesis rate of resin could be obtained and the synthesis rate of B-COPNA resin could be controlled by adjusting operation conditions. This work not only could improve the utilization efficiency of ETLF but also lays a theoretical

foundation for controllably preparing B-COPNA resin, aiming to regulate the performance of carbon materials and extend their industrial applications.

CRediT authorship contribution statement

Yuan-Qin Zhang: Writing – review & editing, Writing – original draft, Data curation. **Ling-Rui Cui:** Writing – review & editing, Data curation. **Hong-Yan Shen:** Data curation. **Jun-Ping Shen:** Data curation. **Hong-Fang Ma:** Methodology, Data curation. **Jun Xu:** Writing – review & editing, **Fa-Hai Cao:** Writing – review & editing, Data curation.

Declaration of competing interest

We declare that we have no financial and personal relationships with other people or organizations that can inappropriately influence our work, there is no professional or other personal interest of any nature or kind in any product, service and/or company that could be construed as influencing our manuscript entitled "Synthesis kinetics of B-COPNA resin monitored by the transformation of functional groups using In-situ FTIR spectroscopy".

Acknowledgement

This research is financially supported by the National Natural Science Foundation of China (52174023), National Natural Science Foundation of P. R. China (22308104), and China Petroleum Engineering Corp., Ltd. (CPEC) (2021ZYGC-01-01). The authors also would like to thank the Research Center of Analysis and Test of East China University of Science and Technology for the help on the characterization of FT-IR spectra.

Appendix A. Supplementary data

Supplementary data to this article can be found online at https://doi.org/10.1016/j.petsci.2025.06.003.

References

Ahmad, T., Manzar, M., Georgin, J., et al., 2023. Development of a new hyper crosslinked resin based on polyamine-isocyanurate for the efficient removal of endocrine disruptor bisphenol-A from water. J. Water Process Eng. 53, 103623. https://doi.org/10.1016/j.jwpe.2023.103623.

Ahmad, T., Manzar, M.S., Khan, S., et al., 2024. Enhanced adsorption of bisphenol-A from water through the application of isocyanurate based hyper crosslinked resin. J. Mol. Liq. 395, 123861. https://doi.org/10.1016/j.molliq.2023.123861.

Chen, R., Guo, Y., Zhang, Y., et al., 2023. Reaction mechanism of ethylene tar in the air atmosphere. Fuel 353, 129146. https://doi.org/10.1016/j.fuel.2023.129146.

Cheng, X., Song, S., 2012. Eutectic effect during mesophase formation in cocarbonization of ethylene tar pitch and polystyrene. Int. J. Min. Sci. Technol. 22 (2), 183–186. https://doi.org/10.1016/j.ijmst.2011.08.008.

Cheng, X., Zhang, M., Wang, Z., et al., 2018. IR and kinetic study of sewage sludge combustion at different oxygen concentrations. Waste Manag. 74, 279–287. https://doi.org/10.1016/j.wasman.2018.01.005.

Fang, W., Cui, L., Zhang, Y., et al., 2022. Investigation on a novel preparation process of B-COPNA resin from catalytic cracking diesel. Fuel 320, 123916. https://doi. org/10.1016/j.fuel.2022.123916.

Fujitsuka, H., Yamaji, M., Nakatani, R., et al., 2024. Metal-assisted low-temperature cracking of n-hexane over Rh-encapsulated ZSM-5 catalysts. Microporous Mesoporous Mater. 376, 113199. https://doi.org/10.1016/j.micromeso.2024. 113199.

Ge, C.Z., Yang, H.X., Wang, J.T., et al., 2016. Highly effective utilization of ethylene tar for mesophase development via a molecular fractionation process. RSC Adv. 6 (1), 796–804. https://doi.org/10.1039/c5ra20651k.

Guo, J., Lu, S., Xie, J., et al., 2023. Preparation of mesophase pitch with domain textures by molecular regulation of ethylene tar pitch for boosting the performance of its carbon materials. J. Anal. Appl. Pyrolysis 170, 105932. https:// doi.org/10.1016/j.jaap.2023.105932.

Kusakabe, K., Gohgi, S., Morooka, S., 1998. Carbon molecular sieving membranes derived from condensed polynuclear aromatic (COPNA) resins for gas

- separations. Ind. Eng. Chem. Res. 37 (11), 4262–4266. https://doi.org/10.1021/ie9804024
- Liang, D., Liu, D., Yang, S., et al., 2020. Effects of bromination-dehydrobromination on the microstructure of isotropic pitch precursors for carbon fibers. Polymers 12 (12), 3059. https://doi.org/10.3390/polym12123059.
- Lin, Q., Zheng, M., Qin, T., et al., 2010a. Preparation of solid carbon spheres by pyrolysis of allyl COPNA-BMI resin. J. Anal. Appl. Pyrolysis 89 (1), 112–116. https://doi.org/10.1016/j.jaap.2010.06.005.
- Lin, Q., Zheng, R., Tian, P., 2010b. Preparation and characterization of BMI resin/graphite oxide nanocomposites. Polym. Test. 29 (5), 537–543. https://doi.org/10.1016/j.polymertesting.2010.01.007.
- Liu, D., Lou, B., Chang, G., et al., 2018a. Study on effect of cross-linked structures induced by oxidative treatment of aromatic hydrocarbon oil on subsequent carbonized behaviors. Fuel 231, 495–506. https://doi.org/10.1016/j. fuel.2018.05.122.
- Liu, H., Lin, Q., Li, Y., et al., 2014. Preparation of near net-shape carbon foams from allyl COPNA-modified bismaleimide resin. J. Anal. Appl. Pyrolysis 110, 476–480. https://doi.org/10.1016/j.jaap.2014.10.019.
- Liu, J., Chen, X., Xie, Q., et al., 2020. Controllable synthesis of isotropic pitch precursor for general purpose carbon fiber using waste ethylene tar via bromination-dehydrobromination. J. Clean. Prod. 271, 122498. https://doi.org/ 10.1016/j.iclepro.2020.122498.
- Liu, J., Li, Y., Shen, C., et al., 2022. Controllable synthesis of a carbonaceous pitch from molecular dimension by a novel method of chlorination-dechlorination. Fuel 326, 125132. https://doi.org/10.1016/j.fuel.2022.125132.
- Liu, J., Shen, C., Huang, L., et al., 2023. Preparation of pitch precursor with excellent spinnability for general-purpose carbon fibre using coal tar pitch as raw material. Chin. J. Chem. Eng. 54, 22–28. https://doi.org/10.1016/j.cjche.2022.01.003.
- Liu, J., Shimanoe, H., Nakabayashi, K., et al., 2018b. Enhancing the oxidative stabilization of isotropic pitch precursors prepared through the co-carbonization of ethylene bottom oil and polyvinyl chloride. J. Ind. Eng. Chem. 67, 358–364. https://doi.org/10.1016/j.jiec.2018.07.008.
- Liu, J.C., Shimanoe, H., Nakabayashi, K., et al., 2018c. Preparation of isotropic pitch precursor for pitch-based carbon fiber through the co-carbonization of ethylene bottom oil and polyvinyl chloride. J. Ind. Eng. Chem. 67, 276–283. https://doi.org/10.1016/j.jiec.2018.06.039.
- Muñoz, I., Weidema, B.P., 2024. Ethylene and propylene production from steam cracking in Europe: a consequential perspective. Int. J. Life Cycle Assess. 29, 745–758. https://doi.org/10.1007/s11367-024-02282-1.
- Niu, Z., Liu, G., Yin, H., et al., 2016. In-situ FTIR study of reaction mechanism and chemical kinetics of a Xundian lignite during non-isothermal low temperature pyrolysis. Energy Convers. Manag. 124, 180–188. https://doi.org/10.1016/j. enconman.2016.07.019.
- Ota, M., Otani, S., Kobayashi, K., 1989. The preparation and properties of the condensed polynuclear aromatic (COPNA) resins using an aromatic aldehyde as crosslinking agent. Chem. Lett. 18 (7), 1175–1178.
- Ōtani, S., Raskovic, V., Ōya, A., et al., 1986. Some properties of a condensed polynuclear aromatic resin (COPNA) as a binder for carbon fibre composites. J. Mater. Sci. 21 (6), 2027–2032.
- Özsin, G., Pütün, A.E., Nakabayashi, K., et al., 2019. Environmental-friendly production of carbon fiber from isotropic hybrid pitches synthesized from waste biomass and polystyrene with ethylene bottom oil. J. Clean. Prod. 239, 118025. https://doi.org/10.1016/j.jclepro.2019.118025.
- Shen, H., Cui, L., Wei, X., et al., 2024. B-COPNA resin formation from ethylene tar light fractions: process development and mechanical exploration by molecular

- simulation. Chin. J. Chem. Eng. 70, 118–129. https://doi.org/10.1016/j.cjche.2024.03.005.
- Shi, K., Yang, J.X., Ye, C., et al., 2019a. A Comparison of ethylene-tar-derived isotropic pitches prepared by air blowing and nitrogen distillation methods and their carbon fibers. Materials 12 (2), 305. https://doi.org/10.3390/ ma12020305.
- Shi, K., Zhang, X.X., Wu, W., et al., 2019b. Effect of the oxygen content and the functionality of spinnable pitches derived from ethylene tar by distillation on the mechanical properties of carbon fibers. N. Carbon Mater. 34 (1), 84–94. https://doi.org/10.1016/S1872-5805(19)60003-X.
- Shi, Y.Y., Wu, M.B., Wang, Y.W., et al., 2012. Effects of cross-linking agents on synthesis of heat-resistant resin from ethylene tar. Appl. Mech. Mater. 217–219, 1159–1165. https://doi.org/10.4028/www.scientific.net/AMM.217-219.1159.
- Tanemura, K., Suzuki, T., Nishida, Y., et al., 2011. Synthesis of the sulfonated condensed polynuclear aromatic (S-COPNA) resins as strong protonic acids. Tetrahedron 67 (6), 1314–1319. https://doi.org/10.1016/j.tet.2010.11.077.
- Tokunaga, A., Shundo, A., Kuwahara, R., et al., 2024. Effect of number density of epoxy functional groups on reaction kinetics for epoxy resin. Macromolecules 57 (22), 10530–10538. https://doi.org/10.1021/acs.macromol.4c02178.

 Tomazett, V.K., Santos, W.G., Lima-Neto, B.S., 2017. Infrared spectroscopy as an
- Tomazett, V.K., Santos, W.G., Lima-Neto, B.S., 2017. Infrared spectroscopy as an effective tool in ring-opening metathesis polymerization: monitoring the polymerization kinetics of norbornene with amine-based Ru catalysts in real time. React. Kinet. Mech. Catal. 120, 663–672. https://doi.org/10.1007/s11144-017-1147-5
- Wang, H., Yang, J., Li, J., et al., 2019. Effects of oxygen content of pitch precursors on the porous texture and surface chemistry of pitch-based activated carbon fibers. SN Appl. Sci. 1 (3), 248. https://doi.org/10.1007/s42452-019-0282-1.
- Wang, K., Li, Y., Zhang, K., et al., 2016. Preparation of near net-shape carbon foams from allyl COPNA-modified bismaleimide resin: structures and properties. J. Anal. Appl. Pyrolysis 117, 125–131. https://doi.org/10.1016/j.jaap.2015.12.006.
- Wu, M.B., Wei, J., Wang, Y.W., et al., 2013. Synthesis of condensed polynuclear aromatic resin from furfural extract oil of reduced-pressure route II. Pet. Sci. 10 (4), 584–588. https://doi.org/10.1007/s12182-013-0310-5.
- Wu, M.B., Wang, Y.W., Wei, J., et al., 2014. Improvements of heat resistance and adhesive property of condensed poly-nuclear aromatic resin via epoxy resin modification. Pet. Sci. 11 (4), 578–583. https://doi.org/10.1007/s12182-014-0374-x.
- Wu, M.B., Shi, Y.Y., Li, S.B., et al., 2012. Synthesis and characterization of condensed polynuclear aromatic resin derived from ethylene tar. China Pet. Process. Petrochem. Technol. 14 (4), 42–47.
- Xing, Y., Wang, Y., Huang, J., et al., 2020. Study on the mechanism and kinetics of waste polypropylene cracking oxidation over the Mn₂O₃/HY catalyst by TG-MS and in situ FTIR. Ind. Eng. Chem. Res. 59 (38), 16569–16578. https://doi.org/ 10.1021/acs.iecr.0c02678.
- Ye, S., Yang, S., Ni, L., et al., 2022. Mechanism and kinetic study of Paal-Knorr reaction based on in-situ MIR monitoring. Spectrochim. Acta Mol. Biomol. Spectrosc. 264, 120280. https://doi.org/10.1016/j.saa.2021.120280.
- Yu, Y., Wang, F., Biney, B.W., et al., 2022. Co-carbonization of ethylene tar and fluid catalytic cracking decant oil: development of high-quality needle coke feedstock. Fuel 322, 124170. https://doi.org/10.1016/j.fuel.2022.124170.
- Zhang, G.L., Ke, Y.C., Qin, M.R., et al., 2015. Preparations and tribological properties of COPNA copolymer materials. Procedia Eng. 102, 615–624.
- Zhang, Y., Wang, J., Xue, S., et al., 2016. Kinetic study on changes in methyl and methylene groups during low-temperature oxidation of coal via in-situ FTIR. Int. J. Coal Geol. 154–155, 155–164. https://doi.org/10.1016/j.coal.2016. 01.002.